

FACILITY FORM 602-1
N 66-11210

(ACCESSION NUMBER)

25
(PAGES)

(THRU)

(CODE)

(CATEGORY)

X-614-65-289

NASA TM X-55314

**ON THE DETERMINATION OF
SOLAR EUV EMISSION ALTITUDES
USING THE EARTH
AS AN OCCULTING DISK**

BY

S. O. KASTNER

C. L. WOLFF

GPO PRICE \$ _____

CFSTI PRICE(S) \$ _____

Hard copy (HC) 1.00

Microfiche (MF) 50

ff 653 July 65

JULY 1965



GODDARD SPACE FLIGHT CENTER
GREENBELT, MARYLAND

ON THE DETERMINATION OF SOLAR EUV EMISSION ALTITUDES
USING THE EARTH AS AN OCCULTING DISK

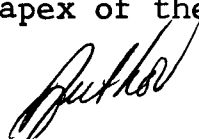
By

S. O. Kastner and C. L. Wolff
Goddard Space Flight Center
Greenbelt, Maryland

ABSTRACT

11210
A possible method of determining the altitudes in the solar atmosphere at which various EUV emission lines originate is discussed. The method makes use of the earth as an occulting disk to obscure the solar disk and steadily changing amounts of the inner corona and chromosphere. With proper choice of trajectories for a spacecraft, about 10 hours of observing time from within the earth's shadow may be obtained.

The variation in intensity of chromospheric emission lines, due to partial eclipse by the earth, is calculated along trajectories within the earth's umbra. The emission lines are assumed to originate in spherical shells and have a gaussian distribution of intensity about a height of maximum intensity. It is verified that discrimination is possible between several emission lines originating at altitudes above the photosphere differing by less than 10,000 km. Discrimination is most clear cut if the spacecraft is sent well out toward the apex of the earth's shadow cone.



INTRODUCTION

The extreme ultraviolet (EUV) solar spectrum contains a wealth of lines, due to highly ionized atoms in the chromosphere and corona, a great many of which have not been spectroscopically assigned. Because the ionization and excitation depends on temperature and electron density, the different emissions originate at different levels in the solar atmosphere. Thus, for example, a schematic diagram of Tousey¹ shows a difference in heights of about 10,000 km between BIII and Ne VIII.

Several authors have proposed a steeper temperature gradient than is depicted by Tousey, as summarized by De Jager²; in most of these models coronal temperatures of 10^6 °K are reached at a height of about 10,000 km. On the other hand, some Russian authors³ obtain a more gradual rise, not reaching 10^6 °K before a height of about 20,000 km. The difference between the predominant heights of the various ions will depend upon the steepness of the temperature rise. The existence of spicules, with a different distribution from the interspicule medium, means that the differentiation will not be as pronounced as for a uniform atmosphere. Some differentiation may still be expected to exist, however, which might be utilized to separate the observed emission lines into groups, facilitating their identification, and to throw further light on the chromospheric temperature structure.

In this note we examine an unorthodox approach to this question; namely, the possibility of using a spacecraft-mounted instrument scanning in wavelength to study the variation of EUV emission line intensities as the spacecraft moves along a trajectory in the earth's shadow. The spectrometer is assumed to have a field of view great enough to accept radiation from the corona out to several solar radii, when centered on the sun.

Since visible wavelengths are not absorbed appreciably in the earth's atmosphere, the earth will, of course, not serve as a good occulting disk in the visible. However, it should be a good occulting disk for far ultraviolet wavelengths, since these are strongly absorbed; also, the continuum intensity of the sun's disk is small in the far ultraviolet, as compared to many chromospheric or coronal emission line intensities. This should be true also at x-ray wavelengths. Here we will assume that the earth is an occulting disk with sharply defined edges for EUV light. In later work this assumption will be more carefully examined.

As the observation point (spacecraft) moves out in the earth's shadow, deeper parts of the chromosphere are exposed successively so that any ultraviolet lines primarily emitted in these parts will appear and intensify. The rate of intensification may be expected to be different for groups of emission lines predominating at different levels in the

solar atmosphere. Curves of total emission vs time would be obtained for each emission line in this way. The method is somewhat analogous to the study of the atmospheres of eclipsing binary stars by the variations in their spectra during the cycle.

In this exploratory study we ignore the complications introduced by centers of activity and ray structure, assuming heliocentric symmetry for the emission source distributions. The corona is assumed to be optically thin. Our objective is to find what degree of spatial discrimination between different altitudes of emission can be achieved along possible spacecraft trajectories.

In Section 1, we discuss a family of approximate trajectories and several exact trajectories in order to find how long a spacecraft could remain within the shadow to make useful observations. The emissions visible at any point on these trajectories are calculated in Section 2, assuming simple spherical distributions for the sources. The problems involved in dealing with actual asymmetric sources are briefly touched upon.

Section 1

Spacecraft Trajectories

To study the distribution of coronal emission as a function of altitude above the solar surface, one would like an occulting disk centered on the sun and steadily decreasing in size. This

would be obtained, using the earth as the occulting disk, for a spacecraft which moved radially away from the earth along the axis of the earth's shadow. Such a trajectory is not possible in unpowered flight, but there do exist many unpowered trajectories which traverse considerable fractions of the earth's umbra (lengths in excess of 200,000 km) and remain in the umbra for periods of 10 hours or more. In the appendix we demonstrate this analytically by deriving a family of approximate trajectories in the ecliptic plane which are tangent to the earth's shadow axis.

These trajectories exist over a wide range of energies and points of tangency and the distance traversed within the earth's shadow is not a strong function of these parameters. This is illustrated in Figure A1 of the appendix where the locations of entry to and exit from the shadow are plotted for some typical conditions. The distance, A , of the point of tangency from the center of the earth is given in astronomical units (1.496×10^8 km). The units of E are the customary ones used in the restricted three body problem--in the present instance, 8.9×10^{12} ergs/gram.

Having shown that many suitable trajectories exist, it will be sufficient to select several typical ones to illustrate the kind of altitude discrimination obtainable. In what follows we make use of 6 exact trajectories calculated with an electronic

computer. Three points of tangency were chosen ($A = .007, .008, .009$) and two energies at each point ($E = .002$ and $.05$). Those portions of these trajectories which are near the earth's shadow are shown in Figure 1 where the vertical scale has been amplified for clarity. The approximate durations in the shadow and the altitudes of injection (closest approach to the earth) for each trajectory are given in Table I.

TABLE I

Trajectory		Duration In Shadow (hours)	Altitude of Injection (km)
$E = 0.002$	$A = 0.009$	12	1.0×10^5
	$A = 0.008$	26	0.75×10^5
	$A = 0.007$	34	0.50×10^5
$E = 0.05$	$A = 0.009$	8.1	0.33×10^5
	$A = 0.008$	13.5	0.27×10^5
	$A = 0.007$	16	0.19×10^5

Injection into such trajectories seems possible, even though the injection altitudes for the lower energy trajectories are rather high (80,000 km). The lower energy, $E = .002$, is well within present capabilities--being less than the energy necessary to reach Mars' orbit. The higher energy, however, could take a spacecraft slightly beyond Jupiter's orbit.

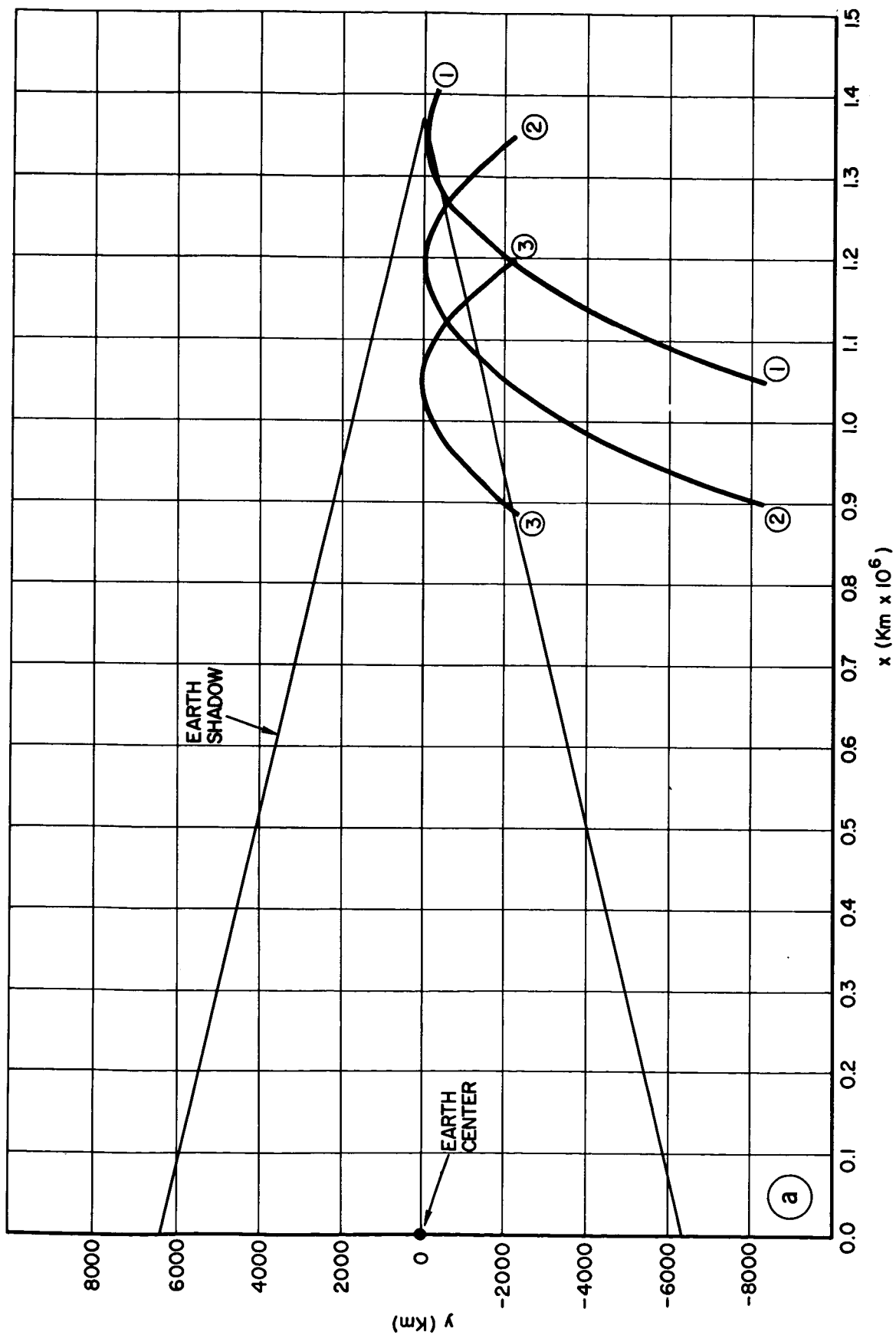


FIGURE 1. (a) Trajectories for $E = 0.002$; (1) $A = 0.009$
 (2) $A = 0.008$
 (3) $A = 0.007$

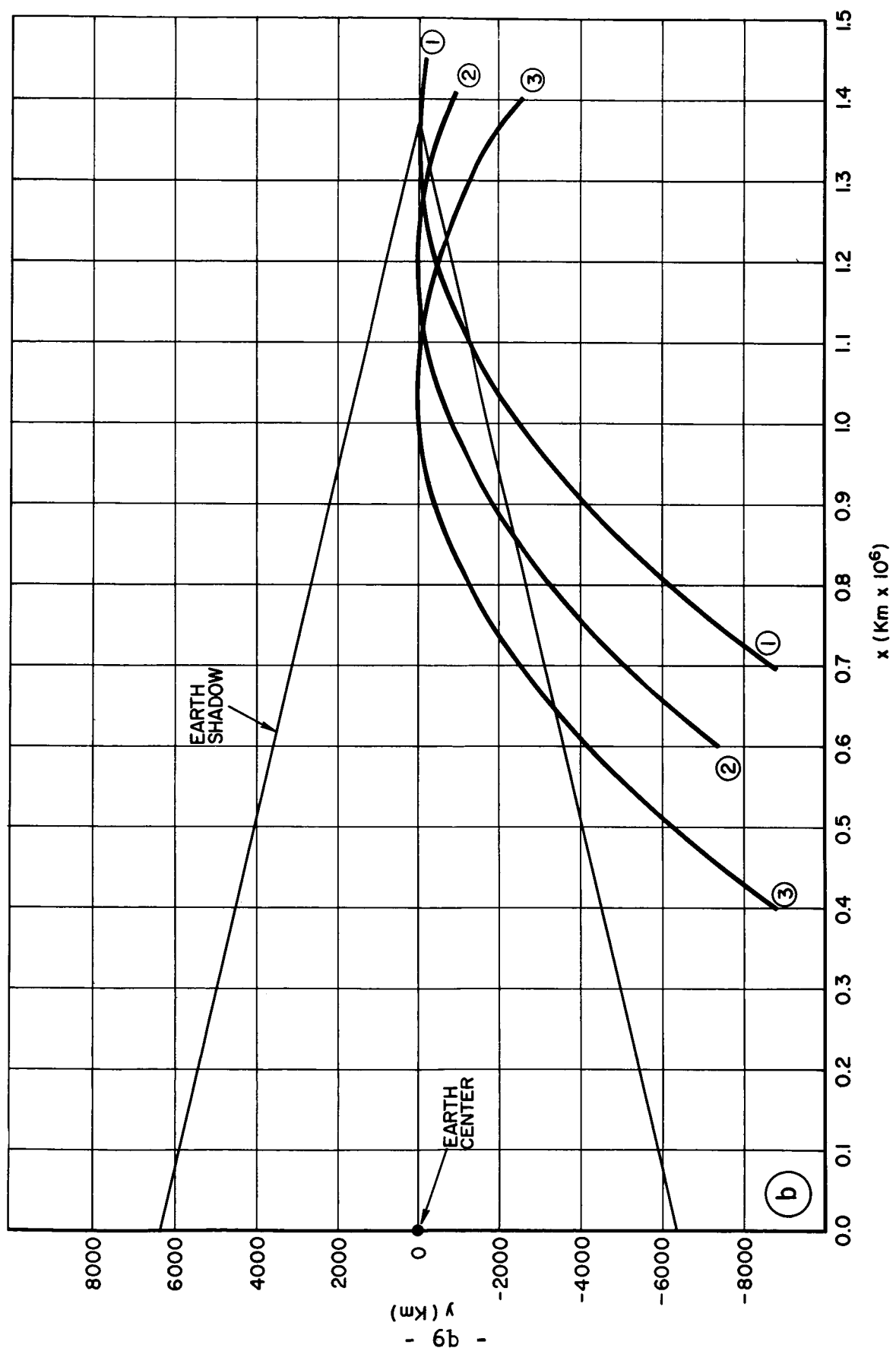


FIGURE 1. (b) Trajectories for $E = 0.05$; (1) $A = 0.009$
 (2) $A = 0.008$
 (3) $A = 0.007$

Section 2

Eclipsing of Coronal Shells

A spherical coordinate system is chosen with origin at sun's center, polar axis along the sun-earth line, and the $\varphi = 0$, $\theta = 90^\circ$ direction toward the north ecliptic pole. As seen from a spacecraft behind the earth, the volume of the corona (and sun) occulted by the earth is actually a conical section which intersects the $\theta = 90^\circ$ plane in a circle of radius R_0 , whose center is displaced a distance, a , from the origin. R_0 and a depend on the observation point. The axis of the conical section makes in general a small non-zero angle with the polar axis. Little error is involved in approximating the conical section by a cylindrical section parallel to the polar axis which intersects the $\theta = 90^\circ$ plane in the same circle. Fig. 2 illustrates the geometry.

If the emission distribution is $E(r, \theta, \varphi)$, the total emission seen at a given point is given by the triple integral:

$$I = \int_0^{2\pi} \int_{\theta_1(\phi)}^{\theta_2(\phi)} \int_{f(\theta, \phi)}^R E(r, \theta, \phi) r^2 \sin \theta \, dr \, d\theta \, d\phi$$

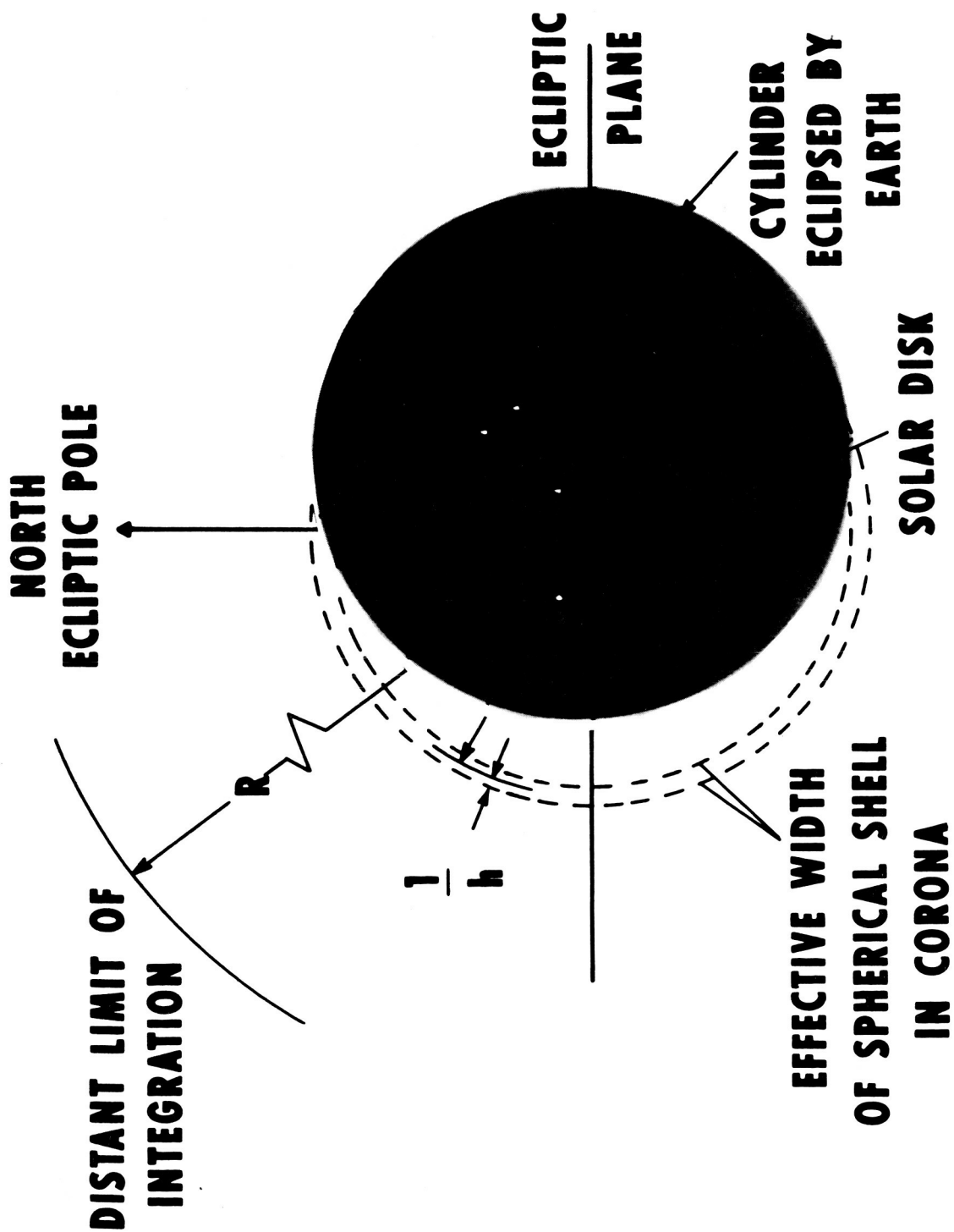


FIGURE 2. Cross-section of plane ($\theta = 90$) through center of sun, as seen from spacecraft

in which $r = f(\theta, \varphi)$ is the equation of the cylinder appropriate to the point of observation, R is an arbitrary radius large compared to the effective extent of the emission source, and the limits $\theta_1(\varphi)$, $\theta_2(\varphi)$ are the intersection curves of the sphere $r = R$ with the cylinder.

To obtain a tractable case we assume a simple model for the coronal emission in a given spectral line, such that it originates in a spherically symmetric shell and has a Gaussian distribution around the peak at $r = r_0$:

$$E(r) = \frac{h}{\sqrt{\pi}} e^{-h^2(r-r_0)^2}$$

The integral becomes, using tables,

$$I = I_1 - I_2 + I_3$$

where

$$I_1 = A \int_0^{2\pi} [\cos \theta_1(\phi) - \cos \theta_2(\phi)] d\phi$$

$$I_2 = B \int_0^{2\pi} \int_{\theta_1(\phi)}^{\theta_2(\phi)} \operatorname{erf} \{h[f(\theta, \phi) - r_0]\} \sin \theta d\theta d\phi$$

$$I_3 = C \int_0^{2\pi} \int_{\theta_1(\phi)}^{\theta_2(\phi)} [f(\theta, \phi) + r_0] e^{-h^2[f(\theta, \phi) - r_0]^2} \sin \theta d\theta d\phi$$

and

$$A = \left(\frac{r_0^2}{2} + \frac{1}{4h^2} \right) \operatorname{erf} \{ h(R-r_0) \} - \left(\frac{R+r_0}{2h\sqrt{\pi}} \right) e^{-h^2(R-r_0)^2}$$

$$B = \left(\frac{r_0^2}{2} + \frac{1}{4h^2} \right)$$

$$C = 1 / 2h\sqrt{\pi}$$

$$f(\theta, \phi) = \left[a \cos \theta + (a^2 \cos^2 \phi - a^2 + R_0^2)^{\frac{1}{2}} \right] / \sin \theta$$

The integrals were evaluated numerically for given values of the input parameters r_0 , h , R and the cylinder radius a and off-axis distance R_0 . (See Fig. 2) The behaviour of the total emission I is shown in Figure 3, for three different source shells along two of the six trajectories discussed in section 1. (b). The three shells, all of the same effective "half-width" $1/h = 2000$ km, have their maxima at heights of 10,000 km, 20,000 km and 30,000 km respectively above the solar surface; they would correspond roughly to the emissions of B III, O VI and Si XII in Tousey's¹ schematic model if that were taken literally.

We note in advance how critically the received emission depends on the shell heights, along trajectory, ($E = 0.002$, $A = 0.009$).

These Gaussian shells drop off much more rapidly with increasing radial distance than typical forbidden line emissions

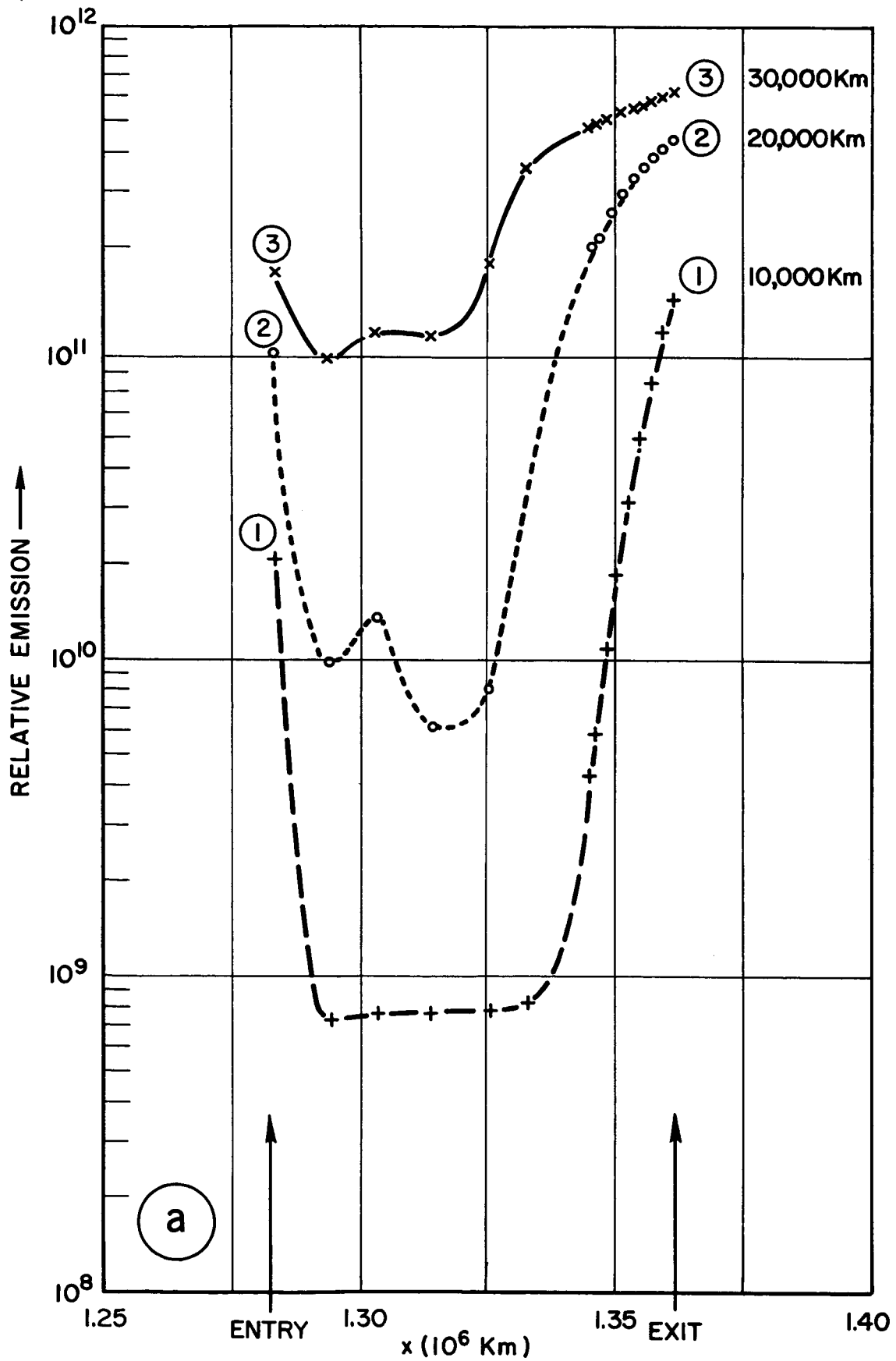


FIGURE 3. (a) Emission curves on trajectory $E = 0.002$,
 $A = 0.009$; (1) shell height 10,000 km,
 (2) shell height 20,000 km,
 (3) shell height 30,000 km

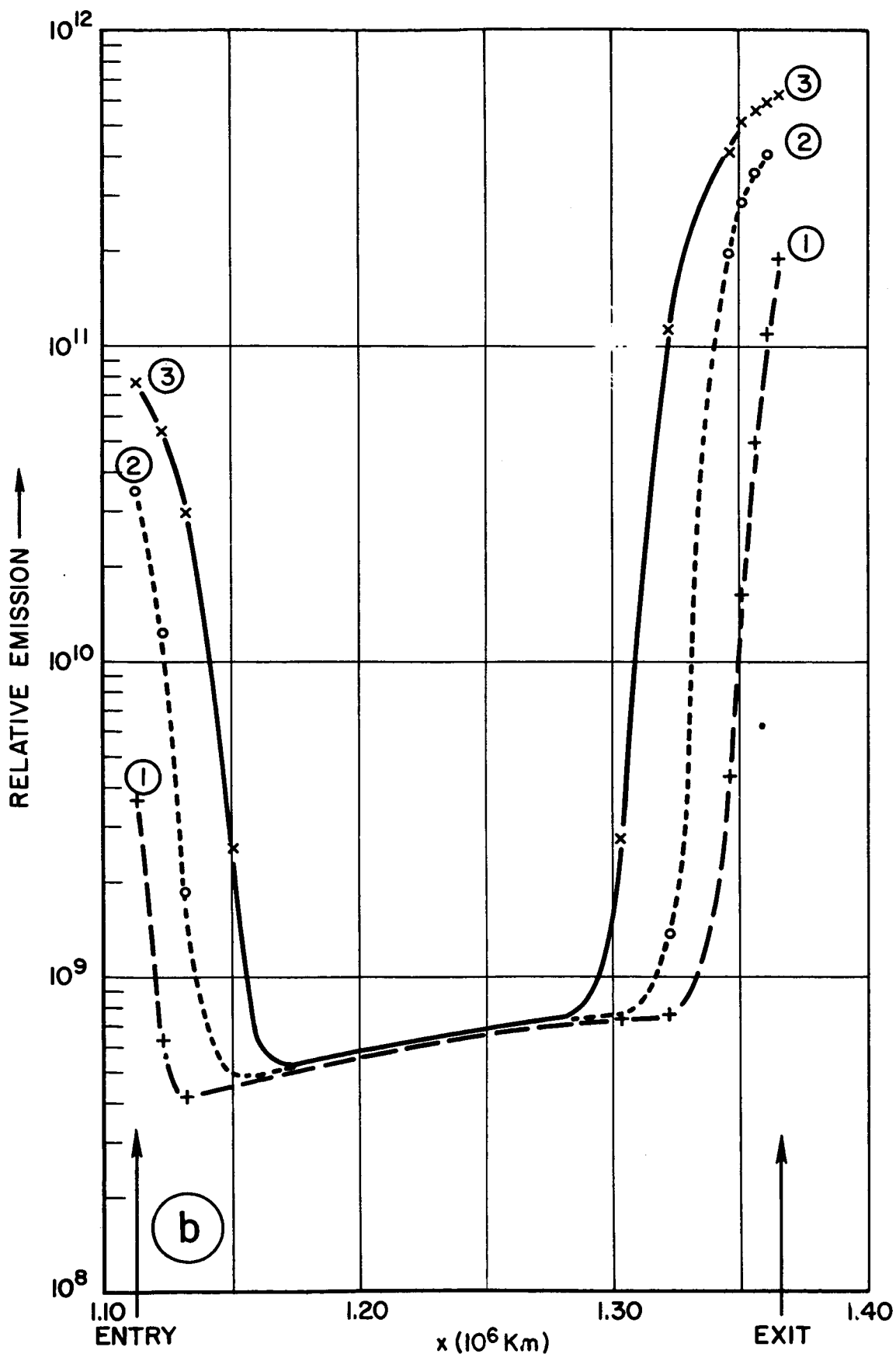


FIGURE 3. (b) Emission curves on trajectory $E = 0.05$,
 $A = 0.009$;

in the visible which are fitted (over a limited range) by exponentials or sums of exponentials. Pottasch⁴ gives

$$\epsilon = (1.14 \times 10^{-7}) \exp\{3 \times 10^{-10} H\} + (0.78 \times 10^{-8}) \exp\{1.3 \times 10^{-10} H\}$$

as the dependence of $\lambda 5303$ on height H . For a height of 10^5 km this function drops to 0.095 of its value at zero height, whereas the Gaussian shell drops to practically zero at 10^5 km from its peak. The comparison must of course be qualified by the fact that the shell has a peak value for $H > 0$, unlike the experimentally derived exponential. We explore the effect of the differences in the next section, however, and find that they do not significantly affect our general conclusions.

DISCUSSION

Referring to figure 3, the difference between the emission curves of source shells 1, 2 and 3 is great along trajectory ($E = 0.002$, $A = 0.009$) which penetrates the earth's shadow only near its very end. The "unclipsed" emission is about 0.15×10^{13} for each shell, in the arbitrary units of figure 3, so that for example the emission from shell 1 is diminished by about four orders of magnitude along trajectory ($E = 0.002$, $A = 0.009$). Near the exit and entry points of the more flattened trajectory ($E = 0.05$, $A = 0.009$) there is also discrimination, but the emission curves practically coincide over most of the range. Along the other 4 trajectories ($A = .007$, and $.008$) virtually no discrimination appears. We can conclude then that there is discrimination only when

the spacecraft is near the apex of the shadow or near its edge. Though these results could have been expected a priori, it is felt to be of value to exhibit them quantitatively.

The secondary minima existing in some of the emission curves are somewhat unexpected. The question arises as to whether these minima would exist for a distribution more like the exponential given by Pottasch. We established that this was so by superposing gaussian shells to give approximately constant emission from the solar surface outward to the position of the maximum of the original gaussian. The decrease of emission from this point outward was the same as before. Emission received at the observation point was essentially unchanged from that given in Figure 3, showing that the secondary minima result from the outward tail of the gaussian only. The number and magnitude of these secondary minima must depend very critically on the kind of shell, e.g. for a spherically asymmetric shell one would expect quite different behaviour. This "fine structure" may thus be an additional aid in deriving the form of the source shell.

Actual emission sources of course depart from spherical symmetry to a greater or lesser extent, requiring the evaluation of more complicated integrals. A helpful feature is that the emission from a complex distribution may be expressed as the sum of emissions from its parts, which may be more conveniently chosen for purposes of integration.

The choice of a trial source distribution would be facilitated by knowledge of existing active regions on the sun, at the time of flight.

As mentioned in section 2, actual emission sources may decrease more slowly with radial distance than do the model shells. This will have two effects; one is to increase the emission seen when the spacecraft is closer to the earth, the other is to decrease the variation in emission along the trajectory and, perhaps, the ability to discriminate. The relative importance of these two effects would vary with actual emission distributions. The general conclusions we have shown above, however, would not be qualitatively changed.

The important question of how much extreme ultraviolet radiation is scattered by the earth's atmosphere to the observation point from the occulted part of the chromosphere will be examined in later work. However rough arguments, considering scattering to occur in a uniform belt of upper atmosphere 100 miles thick in which the scattering efficiency is 100%, indicate that this scattered radiation can compete with direct coronal light only if all but 10^{-4} of the chromospheric emission is eclipsed.

SUMMARY

Flight of spacecraft-borne instruments into the earth's shadow is proposed as a method for obtaining source distributions of ultraviolet and x-ray emission in the corona and chromosphere. Typical trajectories are found to give durations of many hours

and distances of a few hundred thousand km within the shadow. The variation of chromospheric emission along these trajectories is studied for three simple source models. Good discrimination between the three sources is obtained along trajectories whose entry and exit points are farthest toward the end of the shadow.

ACKNOWLEDGMENT

We would like to thank Dr. H. Horstman for a useful discussion and C. Wade for programming the calculations.

REFERENCES

1. Tousey, R., - Science 134, 441 (1961).
2. De Jager, C., - Handbuch der Physik, v.LII, p 142, Springer.
3. Gulyaev, Nikol'sksya and Nikol'skii - Soviet Astronomy
AJ, 7, 332, (1963).
4. Pottasch, S. R., Monthly Notices R.A.S. 125, 543, (1963)
5. Moulton, F. 1914, An Introduction to Celestial Mechanics
p 280, Second Ed., Macmillan.

APPENDIX

Approximate Trajectories in Shadow

Because the umbra of the earth's shadow is so long and thin, any spacecraft trajectory which extends along considerable portions of the shadow length must be of very low curvature and generally parallel to the shadow axis. Such a trajectory is very similar to one which is tangent to the central axis of the shadow. In this Appendix we derive an simple analytic expression for the path of a spacecraft on trajectories tangent to the earth's shadow axis. The expression is valid within the shadow, except close to the earth, and is derived only for motion in the ecliptic plane.

A cartesian coordinate system in the ecliptic plane, centered on the earth, and rotating once per year will be used. The x-axis is chosen to be along the sun-earth line, extended. The equations of motion of the spacecraft are simplest using the units customary in the Restricted 3-Body Problem, namely:

Unit of Length = one astronomical unit (a.u.) = 1.496×10^{13} cm

Unit of Time = $\frac{1}{2\pi}$ sidereal years = 5.02×10^6 seconds.

The equations of motion are then,⁵

$$\begin{cases} \ddot{x} - 2\dot{y} = (1+x)\left(1 - \frac{1-\mu}{S^3}\right) - \frac{\mu x}{S^3} & (1a.) \\ \ddot{y} + 2\dot{x} = y\left(1 - \frac{1-\mu}{S^3}\right) - \frac{\mu y}{S^3} & (1b.) \end{cases}$$

.where,

$$\begin{aligned} s^2 &= x^2 + y^2 \\ s^2 &= (1+x)^2 + y^2 \\ \mu &= 3.039 \times 10^{-6} \end{aligned}$$

The quantity, μ , is the ratio of the mass of the earth-moon system to the mass of the sun. The motion of the moon in its orbit is neglected. Near new moon this will make no qualitative change in the results to be derived. Near full moon, of course, severe perturbations can arise and this Appendix is inapplicable then.

An exact first integral of the equations of motion can be obtained. For any trajectory, this integral is a constant, E , which is the total energy per unit mass of the spacecraft. For brevity, this will be referred to simply as the energy.

$$E = \frac{3}{2} + \frac{\dot{x}^2 + \dot{y}^2}{2} - \frac{S^2}{2} - \frac{1-\mu}{S} - \frac{\mu}{\mathcal{N}} \quad (2.)$$

In this equation, the zero of energy has been chosen so that objects with negative energies are bound to the earth and those with positive values can escape. Numerical values of E may be converted to c.g.s. units by multiplying by the factor 8.9×10^{12} ergs/gram.

To obtain the equation of the trajectory, $y = f(x)$, in the vicinity of the point, $x = A$, where it is tangent to the

x-axis, one more integration must be performed. Use is made of the approximations:

$$y \ll x$$

$$\dot{y} \ll \dot{x}$$

$$\mu \ll 1$$

The first approximation is valid because we will restrict our interest to the more distant half of the earth's shadow.

In this region y is always less than $\frac{1}{200}x$. The second approximation is valid because we are considering orbits of very low curvature which are tangent to the x-axis. Equations 1 and 2 may now be expanded about the point $x = A$. After some algebra, one can derive that:

$$y = -2 \int_A^x dx (x-A) \left[2E + 3x^2 + \frac{2\mu}{x} \right]^{-\frac{1}{2}} \quad (3.)$$

For energies, $E > .004$, the term in square brackets is essentially constant, allowing easy integration:

$$y = \frac{(x-A)^2}{\sqrt{2E}} \quad (4.)$$

Equation (4) is the approximate trajectory desired. The coordinates, x_e , of the entry into and exit from the umbra are then obtained by using the equation of the umbra edge:

$$y = \frac{(.0092 - x)}{217} \quad (5.)$$

Solving equations (4) and (5) simultaneously for x gives,

$$x_e = (A - \gamma) \pm (2\gamma)^{\frac{1}{2}} \left(.0092 - A + \frac{\gamma}{2} \right)^{\frac{1}{2}}$$

where,

$$2\gamma = \frac{\sqrt{2E}}{217}$$

Values of x_e are plotted in figure A-1 for three tangency points, $A = .006, .008, \text{ and } .009 \text{ a.u.}$ Each value of energy determines two values of x_e . The distance between them (entry and exit) is not a strong function of A or E , being typically from $.001$ to $.003 \text{ a.u.}$ or about one quarter the length of the umbra. Thus, for a wide variety of orbits, a spacecraft will move longitudinally along the earth's shadow axis, giving a considerable variation in the eclipsed portion of the solar corona during the course of its flight.

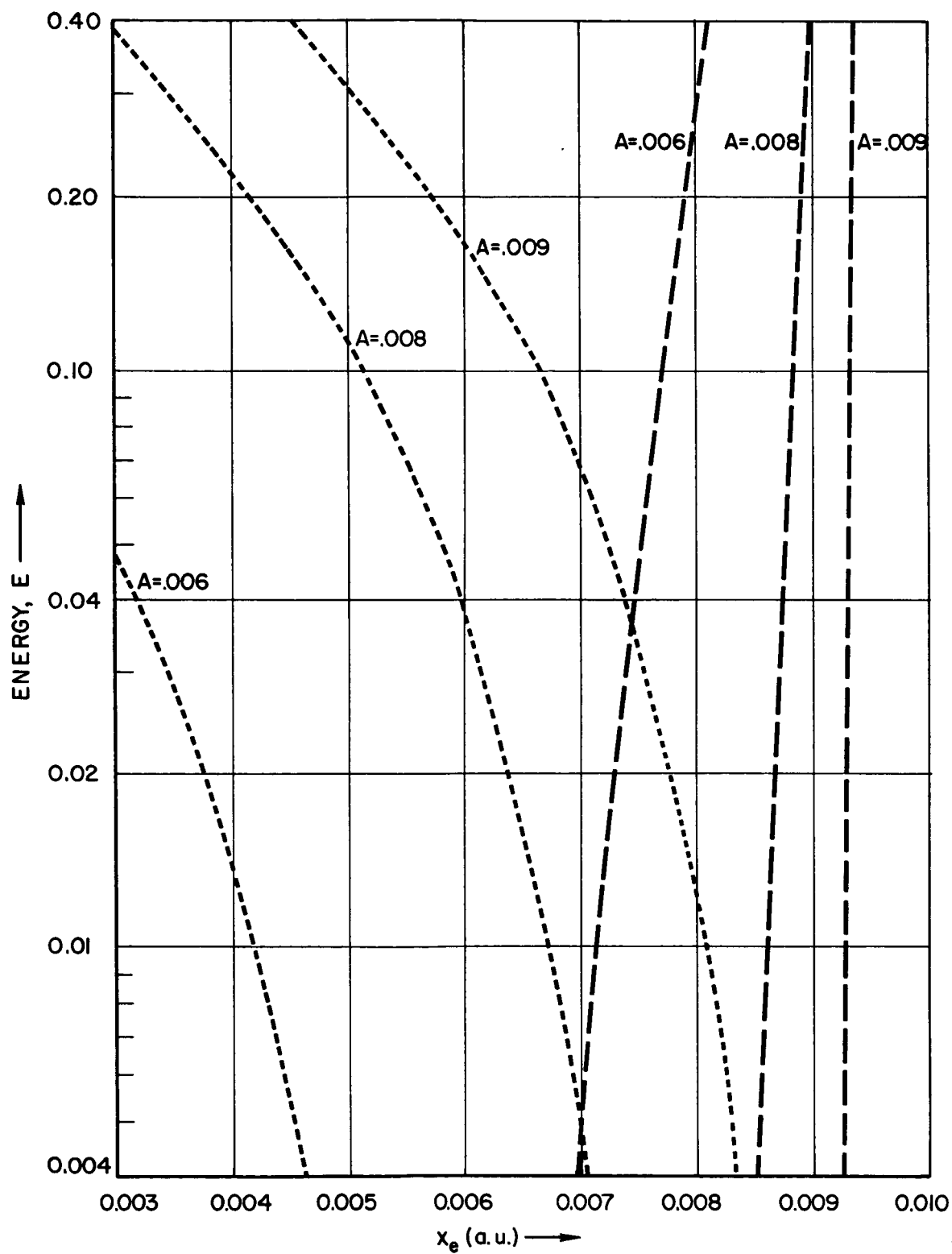


FIGURE A-1. Shadow exit and entry distances; entry curves dotted, exit curves dashed